Journal of The Electrochemical Society, **162** (6) H366-H370 (2015)
0013-4651/2015/162(6)/H366/5/$33.00 © The Electrochemical Society

Photoelectrochemical Hydrogen Generation Using C-dot/ZnO Hierarchical Nanostructure as an Efficient Photoanode

Heejin Kim,[a] Woosung Kwon,[b] Mingi Choi,[a] Shi-Woo Rhee,[b,*] and Kijung Yong[a,*,z]

[a]*Surface Chemistry Laboratory of Electronic Materials, Department of Chemical Engineering, Pohang University of Science and Technology (POSTECH), Pohang 790-784, South Korea*
[b]*Laboratory for Advanced Molecular Processing, Department of Chemical Engineering, Pohang University of Science and Technology (POSTECH), Pohang 790-784, South Korea*

In this study, we have developed a stable and environmental-friendly photoelectrode of carbon nanodots (C-dots) coupled with a 3 dimensional ZnO structure. Our C-dots are synthesized hydrothermally with a high yield of 40%, and they are successfully anchored onto the ZnO backbone via a facile solution procedure. The as-prepared C-dot/ZnO photoelectrodes have exhibited reasonable photocurrent density and remarkable photostability under the 1 sun irradiation condition without any sacrificial reagent. We have studied the chemistry beneath the C-dot/ZnO interface through various spectroscopic and electrochemical techniques. This work could shed light on future application of C-dots in efficient and toxin-free solar water-splitting systems.
 [DOI: 10.1149/2.0751506jes]

Manuscript submitted January 7, 2015; revised manuscript received February 13, 2015. Published March 11, 2015.

Photogenerated hydrogen, particularly from a water-splitting system, has attracted considerable attention as a promising next-generation energy resource. The photoelectrochemical (PEC) system for water splitting requires eco-friendly, stable, and efficient photoelectrodes to convert solar light into a photocurrent.[1–6] Various photoelectrode materials have been investigated, including TiO_2, WO_3, ZnO, and Fe_2O_3.[7–12] In particular, ZnO is regarded as a promising photoelectrode semiconductor material due to its high photoresponsibility, electron mobility, and abundance.[13,14] In addition, 1D ZnO nanostructure arrays facilitate direct electron pathways, resulting in efficient charge separation.[15] However, ZnO has limitations as a photoelectrode material due to its large band-gap, which can only absorb in the UV light region. For this reason, there have been several efforts to enhance the light absorbing capability by employing visible light sensitizers, such as organic dyes[16,17] or low-band-gap semiconductors. However, visible light sensitizers have suffered from low stability despite exhibiting high solar-to-chemical conversion efficiency.

To realize the water-splitting PEC system, high photoelectrode stability is crucial.[18] In this respect, we have developed a carbon nanodot (C-dot) modified ZnO nanostructure photoelectrode for stable and environmental-friendly water-splitting systems. In the past decade, C-dots have been the subject of a number of studies, ranging from synthetic methodology to practical applications, typically as biocompatible imaging agents or phosphorous.[19] Few papers have previously reported the PEC use of C-dots as light harvesters,[19–21] inspired either by efficient exciton generation from visible light absorption or by the near lack of intrinsic toxicity compared to cadmium- or lead-containing quantum dots.[23,24] However, several difficulties have been encountered in exploiting C-dots in actual PEC cells, particularly due to the poor durability arising from the "bare" (or unpassivated) surface of C-dots and the energy level mismatch buried in the oxygen evolution reaction, which leads to the inevitable use of a sacrificial electrolyte.

To overcome the limitations of these previous approaches, we were intrigued by the feasibility of utilizing amine-passivated C-dots. In this study, the obtained photoelectrochemical properties which can be represented by the hydrogen generation rate was 0.43 umol/$cm^2 \cdot$ min. Although this value is hard to compare exactly with other previous research because the H_2 generation condition system is not equal such as electrolyte, pH condition, applied potential values, and light absorbing capability, this value is comparable with that of the other hydrogen generation C-dot sensitized TiO_2 nanotube (0.43 umol/$cm^2 \cdot$ min at 0 V vs. Ag/AgCl with sacrificial reagent)[22] and TiO_2 nanotube array photoelectrochemical cells with 0.013 umol/ $cm^2 \cdot$ min.[7] The surface amine groups are expected to constitute a powerful shield protecting the core against undesired oxidation and allow us to adjust the energy level through the auxochromic effect.[19] We now report the design and demonstration of a ZnO nanostructure-based PEC system sensitized with the amine-passivated C-dots.

Experimental

Fabrication of 3D ZnO photoelectrode.— The ZnO nanostructure consists of a 1D ZnO nanowire (core) and 2D ZnO nanosheets on the nanowire surface to enhance the effective surface area for C-dot sensitizing. For the photoelectrode, the ZnO nanowire arrays were first synthesized using the hydrothermal method on fluorine-doped tin oxide (FTO) glass at 95°C.[25,26] Briefly, the ZnO pre-sputtered FTO glass was immersed in 10 mM $Zn(NO_3)_3 \cdot 6H_2O$ (98%, Aldrich) aqueous solution adjusted to pH 11 with ammonia solution. The solution was maintained at 95°C overnight. Then, for secondary growth on the ZnO nanowire arrays, the samples were reacted in equal molecular amounts of 10 mM $Zn(NO_3)_3 \cdot 6H_2O$, hexamethylenediamine ($C_6H_{16}N_2$, Aldrich), and 1 mM trisodium citrate ($C_6H_5Na_3 \cdot 2H_2O$, Aldrich) at 70°C for various times.

Synthesis of amine-passivated C-dots.— The precursor consists of 1 g of citric acid and 1 mL of 0.5 M nitric acid in 1 mL of water. The mixture was vigorously stirred to dissolve the citric acid and then injected with 1 mL of oleylamine and 9 mL of octadecene. The solution was vigorously stirred for 10 min to form a milky emulsion. The emulsion was heated to 250°C in ambient argon for 2 h. The resulting dark-brown solution was precipitated with methanol, isolated by centrifugation (3,000 rpm for 10 min), and re-dispersed in hexane. This process was repeated three times to remove residuals. The final colloidal C-dots (~1 g) were dried in a vacuum oven (80°C) overnight and then stored in a desiccator for later use. The purified oleylamine-passivated C-dots were ligand exchanged with ethanolamine ($NH_2CH_2CH_2OH$). Ethanolamine was added to a solution of C-dots in toluene (10 mg mL^{-1}) in excess. The mixture was vigorously stirred and heated at 100°C for 12 h.

Fabrication of photoelectrochemical cells.— The previously prepared ZnO nanostructured FTO glass was immersed in a C-dot solution for 24 h to fabricate a C-dot-modified ZnO photoanode. A copper wire was contacted with the photoanode by using silver paste, and consequently heated at 70°C for 1 h. After heating, the photoanode was covered with epoxy except its central active area (0.25 cm^2), and heated again at 70°C for 1 h.

Characterizations.— UV-vis absorption spectra were recorded on a Mecasys Optizen POP spectrophotometer. PL spectra were recorded on a Jasco FP-8500 fluorometer. TEM was performed

*Electrochemical Society Active Member.
[z]E-mail: kyong@postech.ac.kr

using JEOL JEM-2200FS with the image Cs-corrector (accelerating voltage = 200 kV). XPS was performed using an Escalab 250 spectrometer with an Al X-ray source (1486.6 eV). Infrared (IR) spectroscopy was performed using a Nicolet 6700 FT-IR spectrometer. ^{13}C NMR spectra were obtained by Bruker DRX500. Ultraviolet photoelectron spectroscopic measurements with Au-coated silicon substrates were carried out in an ultra-high-vacuum system equipped with a VUV-5000 generator (40.8 eV He II laser) and a SES-100 detector. Kelvin probe analysis was performed with Au-coated silicon substrates by using an SKP5050 Scanning Calvin probe (KP Technology). The photoelectrochemical properties of C-dot/ZnO hierarchical nanostructure were measured using a typical three-electrode potentiostat system (potentiostat/galvanostat, model 263A, EG&G Princeton Applied Research) with Pt flag and Ag/AgCl as counter and reference electrodes, respectively. This system was immersed in phosphate–buffered 0.5 M Na_2SO_4 (pH 7) electrolyte solution, which was purged with N_2 gas for 1 h prior to the measurement. The working electrode with 5×5 mm^2 working area was illuminated from the front side with a solar-simulated light source (AM 1.5 G filtered, 100 mW cm^{-2}, 91160, Oriel).

Results and Discussion

The amine-passivated C-dots were prepared via the soft-template synthesis using citric acid and oleylamine as a precursor and a passivation agent (Figure 1a). Heating the water droplets containing citric acid stabilized by oleylaminium ions in octadecene gives rise to dehydration and carbonization of citric acid, finally resulting in oleylamine-passivated C-dots. Oleylamine, primary amine with a long hydrocarbon tail, hereby plays the key role of suppressing undesirable side reactions (for instance, aggregation between the C-dots), affording the C-dots in an excellent yield of ca. 40% and with uniform size distribution. This intermediate was then subjected to the replacement of oleylamine ligands with ethanolamine. Such ligand-exchanging introduces hydroxide groups in the outermost shell (Figure S1), apparently endowing the C-dots with both water solubility and chemical adsorptivity on metal oxide, without any loss of the inner nitrogen shield. The transmission electron microscopy (TEM) image of the C-dots is shown in Figure 1b, and their mean diameter and standard deviation are 3.5 and 0.26 nm, respectively. Considering the relatively "cold" reaction temperature, it is thought that the C-dots are amorphous or polycrystalline and thus have crystalline carbon (sp^2) domains for internal energy transition within an amorphous carbon matrix.[25] In Figure 1c, the emission map shows that the emission intensity is maximized under 370 nm excitation, which can be attributed to the $n-\pi^*$ transition between the crystalline carbon domains and the surface nitrogen (amine) or oxygen (carbonyl) atoms. The lone pair of electrons of such atoms could reduce the transition energy through the auxochromic effect, and aid the C-dots to absorb visible light. This $n-\pi^*$ transition is responsible for the shoulder observed near 370 nm in the UV-visible spectrum, and the emission peak corresponding to such absorption is observed at 450 nm (Figure 1d). The emission spectra of our C-dots are also dependent upon excitation wavelength, presumably due to the fact that there are various atoms and bondings (or chemical structures) to give diverse transition states, each of which may respond to different photon energies.[27]

Figure 2 shows the scanning electron microscopy (SEM) images of hydrothermally grown ZnO nanowires array and hierarchical 3-dimensional ZnO nanostructures. Firstly, a 1-dimentional ZnO nanowire array was hydrothermally grown on a glass substrate, as shown in Figure 2a. This primary structure was then subject to a secondary growth process to form nanosheet-shaped branches on the surface of the nanowires (Figure 2b). This process was carried out in a citrate ion solution to passivate the polar top planes of the nanowires.

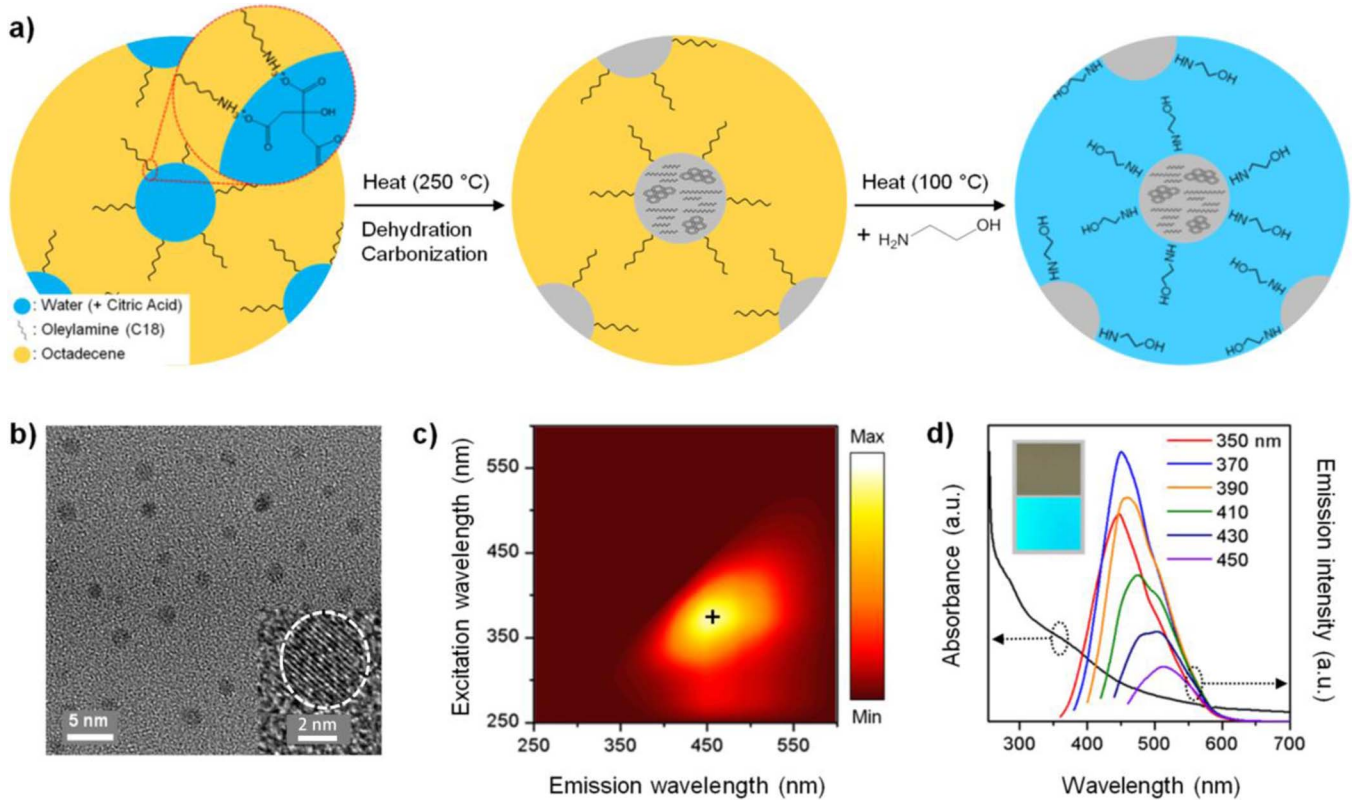

Figure 1. (a) Schematic of the synthesis of nitrogen-passivated C-dots. (b) TEM image of the as-synthesized C-dots, and HR-TEM image of the C-dot (inset). (c) False-color emission map of the C-dots. The black cross marks the position of the maximum emission intensity under 370 nm excitation. (d) UV-visible absorption spectrum (black) and photoluminescence emission spectra under various excitation wavelengths. The color coding represents the excitation wavelength. The inset shows micrographs of the C-dots in water in daylight (top) and under UV light (bottom).

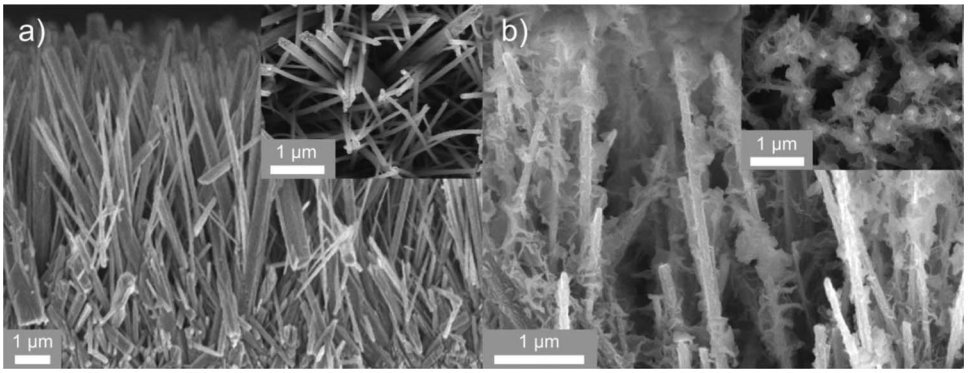

Figure 2. (a) Cross-view and top-view (inset) SEM images of the 1-D ZnO nanowire arrays. (b) Cross-view and top-view (inset) SEM images of the 3-D ZnO nanostructure arrays consisting of 1D ZnO nanowire (core) and 2D ZnO nanosheets on the nanowire surface.

The non-polar side planes of the nanowires became electrochemically negative due to the isoelectric point of ZnO (8.7–9.5) in the citrate ion solution. Thus, the negatively charged citrate ions preferentially adsorbed to the positively charged top planes that were terminated with Zn^{2+}. Due to this capping effect, the growth of the nanowires along the c-axis could be inhibited and nucleation would mostly occur on the side planes of the nanowires during the secondary growth process.

To confirm the C-dot-modified ZnO nanostructure, we performed a high-resolution transmission electron microscopy (HR-TEM) analysis (Figure 3). In the pristine ZnO nanostructure, we can observe that 2D ZnO nanosheets were grown on the nanowire surface (Figure 3a). Electron energy loss spectroscopy (EELS) mapping of Zn and O elements (Figure 3b,c) confirmed the composition of the hierarchical ZnO nanostructure. The interfaces buried in the hierarchical nanostructure is revealed by HR-TEM (Figure 3d), showing that the polycrystalline nanosheets grew sharply on the pre-grown nanowire surface. The formation of polycrystalline nanosheets could be attributed to the fact that they were formed by the aggregation of ZnO nanoparticles assisted by citrate ions in the secondary growth process. With the aid of citrate ions, ZnO nuclei might tend to be adsorbed onto the nanowire sidewall, aggregated with each other, and finally merged to the nanosheets. After our ZnO nanostructure was modified with C-dots (Figure 3e), the EELS maps in Figures 3f-h show the strong signal of carbon on its surface. For further analysis of the C-dot-modified nanostructure, we conducted high-magnification TEM analysis (Figure 3i-k). Magnifying the surface of the nanostructure, we found clear images of C-dots with the lattice spacing of 0.25 nm, corresponding to the (100) facet of graphite carbon.[19] This result might tell us that C-dots were successfully anchored onto the surface of the ZnO nanostructure without any kind of structural deformation or destruction. The adsorption of C-dots was mediated by their hydroxyl groups, forming hydrogen bondings with the ZnO

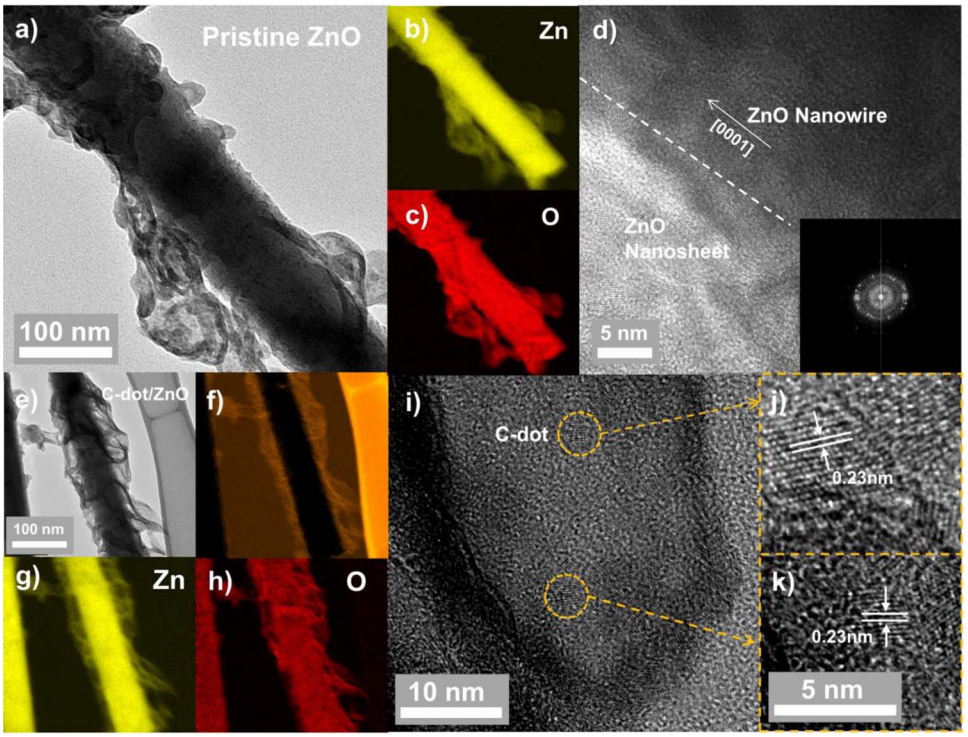

Figure 3. HRTEM images of (a-d) pristine 3D grown ZnO nanostructures and (e-k) C-dot-modified 3D ZnO nanostructures. Low-resolution TEM images of (a) pristine 3D ZnO nanostructures and (e) C-dot-modified ZnO. Electron energy loss spectroscopy (EELS) micrographs of corresponding ZnO with (b) Zn, (c) O and C-dot-modified ZnO with (f) C, (g) Zn, and (h) O. (d) HR-TEM micrograph of 3D ZnO nanostructures at the interface of ZnO nanosheets on a ZnO nanowire core and (inset) reduced fast Fourier transform (FFT) image at the ZnO nanosheet. (i) HR-TEM micrograph of C-dot-modified 3D ZnO in the ZnO nanosheet region and (j, k) magnified TEM image of anchored C-dots with 3.5 nm size.

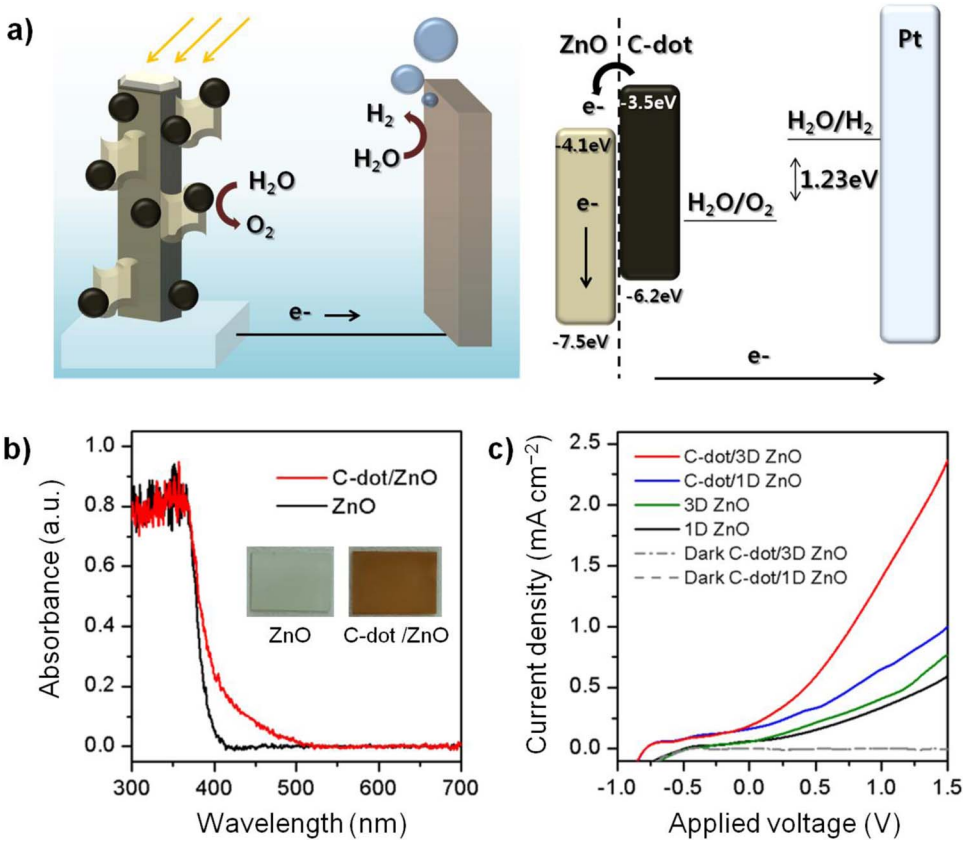

Figure 4. (a) Schematic of the PEC cell system for water splitting using C-dots on the 3D ZnO nanostructure and its working schematic image. (b) Absorption spectra of the 3D ZnO nanostructure and C-dot-modified 3D ZnO nanostructure and the corresponding digital images. (c) Current density versus potential for C-dot-sensitized ZnO nanostructures under illumination of AM 1.5 light at 100 mW/cm^2 with a 5 × 5 mm^2 cell area (0.5 M Na_2SO_4 buffered with phosphate (pH 7)).

surface.[28–30] IR spectroscopy gave qualitative information about the bonding state between C-dots and the ZnO surface (Figure S2). In Figure S2a, the broad band near 3450 cm^{-1} indicated the presence of hydroxyl groups on the ZnO surface. This band was shifted toward lower wavenumbers (3400 cm^{-1}) after the adsorption of C-dots, which could be attributed to the hydrogen bonding between C-dots and the ZnO surface to reduce the bonding energy.

We applied the C-dot-modified ZnO nanostructure to a PEC cell as a photoanode for water splitting (Figure 4a). For solar water-splitting, a 3-electrode PEC system was operated under the 1 sun irradiation condition. The system consists of a C-dot-modified ZnO nanostructure on FTO glass as a working electrode, a Pt mesh as a counter electrode, and a saturated Ag/AgCl electrode as a reference. When the light is illuminated, photoexcited electrons are generated and transported to the Pt counter electrode. The electrons on the Pt counter electrode are then used for water reduction with hydrogen generation. The remaining holes at the working electrode facilitate water oxidation. For this reason, adequate band-gap alignment between the working electrode and the reduction potential for water oxidation is important for designing these PEC cells. As shown in the schematic diagram demonstrating band-gap alignment, the C-dots have adequate valence band and conduction band positions. The valence band level and the Fermi level of the C-dots were estimated by means of ultraviolet photoelectron spectroscopy (UPS) and Kelvin probe analysis, respectively. The valence band obtained is 6.1 eV with the Fermi level of 4.8 eV, which is more negative than the water oxidation potential level (Figure S3). The conduction band was then calculated based on the valence band value and optical absorption property. Because C-dots have multiple band-gap energies with various optical properties, the band-gap for this scheme was determined according to the high-intensity absorption values near 450 nm. As depicted in Figure 4a, the C-dots can generate photoexcited electrons under irradiation and separate electron hole pairs with a cascade band structure using ZnO.

Our C-dots can absorb in the visible light region with an edge of approximately 500 nm in wavelength, as illustrated in Figure 1d. Correspondingly, the C-dot-modified ZnO nanostructure also exhibited a ∼500 nm absorption edge (Figure 4b). To confirm their efficiency as photoelectrodes, PEC analysis was performed in 0.5 M Na_2SO_4 electrolyte (pH 7) under 1 sun illumination. As shown in Figure 4c, the PEC properties were enhanced with C-dot-modified ZnO nanostructures compared to those of pristine ZnO nanostructures. In addition, we further compared the two ZnO nanostructures of 1D ZnO nanowire arrays and the 3D ZnO nanostructure. Although the photocurrent densities of the bare ZnO nanostructures in the 1D and 3D structures did not exhibit a considerable difference, the C-dot-modified ZnO nanostructures exhibited considerable differences of almost 4 times more than that of the bare ZnO nanostructured photoelectrochemical cells (C-dot modified ZnO nanostructure: 0.72 mA/cm^2, bare ZnO nanostructure 0.18mA/cm^2 at the potential of 1.23 V vs. RHE) in terms of their photocurrent value and onset potentials. The C-dot-modified 3D ZnO possessed a considerably higher photocurrent density than the C-dot-modified 1D ZnO. The main reason for this result is the increased effective surface area of 3D ZnO for anchoring C-dots, resulting in enhanced light harvesting. In addition, compared to 1D ZnO, the C-dot-modified 3D ZnO exhibited a cathodic shift in the onset potential from –0.550 V to –0.80 V vs. Ag/AgCl. This cathodic shift is due to the surface catalytic properties, which decrease the kinetic barrier for interfacial charge transfer.[31,32] Moreover, in C-dot-modified ZnO nanostructures, the cascade band structure enables efficient charge transfer between C-dots and ZnO nanostructures through their interface due to the C-dot modification.

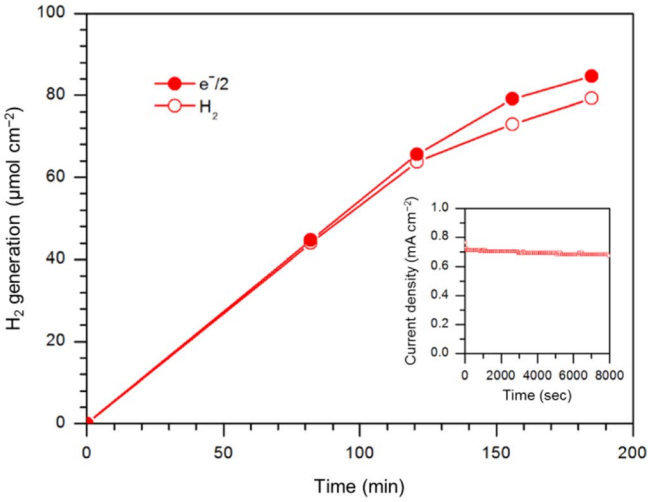

Figure 5. Total hydrogen produced from 1 sun AM 1.5G illumination of C-dot modified 3D ZnO nanostructures, at 1.23 V vs. RHE (empty circles). Also shown is the expected hydrogen evolution calculated from the measured photocurrent assuming 100% faradaic efficiency (filled circles). The inset shows the time-dependent photocurrent density of C-dot modified 3D ZnO photoanode under 1 sun illumination (1.23 V vs. RHE).

In addition to photoelectrochemical current measurements, hydrogen generation was measured at the potential 1.23 V vs. RHE. Figure 5 plots the hydrogen generation of our PEC system as a function of time under 1 sun simulated AM 1.5G illumination. The evolved hydrogen at the Pt counter electrode was collected and analyzed via gas chromatography. The measured hydrogen evolution agreed well with the theoretical calculation assuming 100% faradaic efficiency based on the measured photocurrent density. The obtained hydrogen evolution showed about 93% faradaic efficiency, which indicates that the C-dots prove itself to be a promising material for efficient, stable, and environmental-friendly solar water-splitting systems.

To test the photostability of the C-dot-modified ZnO photoanode, we conducted time-dependent photocurrent density measurements under 1-sun illumination conditions. The applied voltage value was fixed at 1.23 V vs. RHE, which corresponds to the water-splitting potential. As shown in the Figure 5 inset, the photocurrent density was stable for more than 8000 s under 1 sun illumination. Compared to previous studies using light sensitizers,[12,15,31] the results obtained indicate significantly increased stability without the use of sacrificial reagents for the overall water-splitting system. This enhanced stability may come from the amine passivation of the C-dots, which removes surface defect states and constitutes a chemical shield protecting from undesirable oxidation to form strong amide bondings with the intrinsic surface carbonyl groups.[19,27,33]

Conclusions

In summary, we have developed a PEC system for water splitting using a C-dot-modified ZnO nanostructure as the working electrode. The 3D ZnO nanostructure could provide sufficient "sites" for the C-dots to be anchored, leading to efficient PEC performance under 1 sun illumination. The proper energy band structure of our C-dots (especially, their deep valence band level around 6 eV) also realizes hydrogen generation without the use of any kind of sacrificial electrolytes. Also our PEC cells have exhibited excellent stability because the amine passivation of the C-dots could remove surface defect states and constitute a chemical shield protecting their core from undesirable oxidation. These results may pave another way for extending the boundary of the practical use of the C-dots and expedite the development of high-performance environmental-friendly PEC cells for hydrogen generation.

Acknowledgments

This work is supported by the Korea Research Foundation (KRF) under grant No. 2013-R1A2A2A05-005344. Authors Heejin Kim and Woosung Kwon contributed equally.

References

1. D. Gust, T. A. Moore, and A. L. Moore, *Acc. Chem. Res.*, **34**, 40 (2001).
2. S. Khan and J. Akikusa, *J. Phys. Chem. B*, **103**, 7184 (1999).
3. O. Khaselev and J. A. Turner, *Science*, **280**, 425, (1998).
4. N. Chouhan, C. L. Yeh, S. F. Hu, J. H. Huang, C. W. Tsai, R. S. Liu, W. S. Chang, and K. H. Chen, *J. Electrochem. Soc.*, **157**, B1430, (2010).
5. Y. Qiu, K. Yan, H. Deng, and S. Yang, *Nano Lett.*,**12**, 407, (2012).
6. Z. Liu, X. Xie, Q. Xu, S. Guo, N. Li, Y. Chen, and Y. Su, *Electrochimica Acta*, **98**, 268, (2013).
7. G. K. Mor, K. Shankar, M. Paulose, O. K. Varghese, and C. A. Grimes, *Nano Lett.*, **5**, 191 (2005).
8. Y. H. Lu, S. P. Russo, and Y. P. Feng, *Phys. Chem. Chem. Phys.*, **13**, 15973, (2011).
9. J. Su, L. Guo, N. Bao, and C. A. Grimes, *Nano Lett.*, **11**, 1928 (2011).
10. H. Li, C. Cheng, X. Li, J. Liu, C. Guan, Y. Y. Tay, and H. J. Fan, *J. Phys. Chem. C*, **116**, 3802, (2012).
11. K. Sivula , F. Le Formal and M. Grätzel, *ChemSusChem*, **4**, 432, (2011).
12. H. Kim, M. Seol, J. Lee, and K. Yong, *J. Phys. Chem. C*, **115**, 25429, (2011).
13. Y. Bu, Z. Chen, W. Li, and J. Yu, *ACS Appl. Mat. Inter.*, **5**, 5097 (2013).
14. R. Zhang, Q. P. Luo, H. Y. Chen, X. Y. Yu, D. B. Kuang, and C. Y. Su, *ChemPhysChem*, **13**, 1435, (2012).
15. Y. Tak, S. Hong, J. Lee, and K. Yong, *J. Mater. Chem.*, **19**, 5945, (2009).
16. M. Grätzel, Photoelectrochemical cells. *Nature*, **414**, 338 ,(2001).
17. W. J. Youngblood, S. H. A. Lee, Y. Kobayashi, E. A. Hernandez-Pagan, P. G. Hoertz, T. A. Moore, A. L. Moore, D. Gust, and T. E. Mallouk, *J. Am. Chem. Soc.*, **131**, 926, (2009).
18. S. Bensaid, G. Centi, E. Garrone, S. Perathoner, and G. Saracco, *ChemSusChem*, **5**, 500, (2012).
19. W. Kwon and S. W. Rhee, *Chem. Commun.*, **48**, 5256 (2012).
20. N. J. Bell, Y. H. Ng, A. Du, H. Coster, S. C. Smith, and R. Amal, *J. Phys. Chem. C*, **115**, 6004, (2011).
21. L. Han, P. Wang, and S. Dong, *Nanoscale*, **4**, 5814, (2012).
22. X. Zhang, F. Wang, H. Huang, H. Li, X. Han, Y. Liu, and Z. Kang, *Nanoscale*, **5**, 2274, (2013).
23. P. V. Kamat, *J. Phys. Chem. C*, **112**, 18737 (2008).
24. I. Robel, V. Subramanian, M. Kuno, and P. V. Kamat, *J. Am. Chem. Soc.*, **128**, 2385, (2006).
25. H. Kim and K. Yong, *Phys. Chem. Chem. Phys.*, **15**, 2109 (2013).
26. Y. Tak and K. Yong, *J. Phys. Chem. B*, **109**, 19263, (2005).
27. W. Kwon, G. Lee, S. Do, T. Joo, and S. W. Rhee, *Small*, **10**, 506 (2014).
28. B. Meyer and D. Marx, *J. Phys.: Condens. Matter*, **15**, L89 (2003).
29. H. Xu, W. Fan, A. L. Rosa, R. Q. Zhang, and Th. Frauenheim, *Phys. Rev. B*, **79**, 073402, (2009).
30. D. Raymand, A. C. T. van Duin, D. Spāngberg, W. A. Goddard III, and K. Hermansson, *Surf. Sci.*, **604**, 741 (2010).
31. M. Seol, J. Jang, S. Cho, J. Lee, and K. Yong, *Chem. Mater.*, **25**, 184 (2012).
32. J. Li, S. K. Cushing, P. Zheng, F. Meng, D. Chu, and N. Wu, *Nat. Commun.*, **4**, 2651 (2013).
33. Y. P. Sun, B. Zhou, Y. Lin, W. Wang, K. A. S. Fernando, P. Pathak, M. J. Meziani, B. A. Harruff, X. Wang, H. Wang, P. G. Luo, H. Yang, M. E. Kose, B. Chen, L. M. Veca, and S. Y. Xie, *J. Am. Chem. Soc.*, **128**, 7756, (2006).